UCRL-JRNL-229336

LAWRENCE
LIVERMORE
NATIONAL
LABORATORY

Experimental study of radium partitioning between anorthite and melt at 1 atm

S. Miller, D. Burnett, P. Asimow, D. Phinney, I. Hutcheon

March 23, 2007

American Mineralogist

Disclaimer

This document was prepared as an account of work sponsored by an agency of the United States Government. Neither the United States Government nor the University of California nor any of their employees, makes any warranty, express or implied, or assumes any legal liability or responsibility for the accuracy, completeness, or usefulness of any information, apparatus, product, or process disclosed, or represents that its use would not infringe privately owned rights. Reference herein to any specific commercial product, process, or service by trade name, trademark, manufacturer, or otherwise, does not necessarily constitute or imply its endorsement, recommendation, or favoring by the United States Government or the University of California. The views and opinions of authors expressed herein do not necessarily state or reflect those of the United States Government or the University of California, and shall not be used for advertising or product endorsement purposes.

Experimental study of radium partitioning between anorthite and melt at 1 atm

Sarah A. Miller[1*], Donald S. Burnett[1], Paul D. Asimow[1], Douglas L. Phinney[2], and Ian D. Hutcheon[2]

[1]Division of Geological and Planetary Sciences, California Institute of Technology, Pasadena, CA, 91125, U.S.A
[2] Glenn T. Seaborg Institute, Lawrence Livermore National laboratory, Livermore, CA 94551

(Letter manuscript submitted to American Mineralogist February XX, 2007)

ABSTRACT

We present the first experimental radium mineral/melt partitioning data, specifically between anorthite and a CMAS melt at atmospheric pressure. Ion microprobe measurement of coexisting anorthite and glass phases produces a molar D_{Ra} = 0.040±0.006 and D_{Ra}/D_{Ba} = 0.23±0.05 at 1400°C. Our results indicate that lattice strain partitioning models fit the divalent (Ca, Sr, Ba, Ra) partition coefficient data of this study well, supporting previous work on crustal melting and magma chamber dynamics that has relied on such models to approximate radium partitioning behavior in the absence of experimentally determined values.

[*] E-mail: smiller@gps.caltech.edu

INTRODUCTION

Short-lived radioactive isotopes provide unique information about timescales of melting and magma transport processes that operate in the earth's crust and mantle. Any differentiation process that chemically fractionates parent and daughter elements from a decay chain will produce secular disequilibrium in which the activity ratio of the parent and daughter isotopes differs from unity. After approximately five half-lives of the daughter isotope, secular disequilibrium can no longer be measured and the decay rates of the parent and daughter are again equal. Because the half-life of ^{226}Ra is ~1600 years, (^{226}Ra)/(^{230}Th) disequilibria produced within the past 8000 years may be preserved, making it an important chronometer of recent magmatic activity.

Successful interpretation of ^{226}Ra disequilibria in igneous rocks relies on our understanding of its partitioning behavior between minerals and melts. Unfortunately, no stable isotopes of radium exist with which to easily determine such partitioning. Because of the technical challenges involved in conducting experimental partitioning studies with Ra concentrations high enough to be measured *in situ*, our knowledge of Ra partitioning has been restricted to phenocryst/glass analyses of natural rocks producing apparent D_{Ra} values (Cooper et al., 2001) and modeling that either assumes Ra partition coefficients to be comparable to those of barium (e.g., Reagan et al., 1992; Schaefer et al., 1993; Volpe and Hammond, 1991) or employs lattice strain theory and partition coefficients of other divalent elements to approximate D_{Ra} (Blundy and Wood, 1994; 2003)

Partitioning behavior of radium between feldspars and coexisting melts is of particular importance because the large M site of the feldspar structure is one of the few sites in common crustal minerals able to accommodate measurable amounts of Ra, which has an ionic radius of

1.48 Å in VIII-fold coordination (Shannon, 1976). The presence of feldspar potentially can influence ($^{226}Ra/^{230}Th$) disequilibria in magmas generated at pressures below ~1.5 GPa within the plagioclase lherzolite stability field of the upper mantle (Presnall et al., 2002), whether the disequilibria arise from source melting or from diffusive reaction of rising melts with gabbroic cumulates (Saal and Van Orman, 2004; Van Orman et al., 2006). Dufek and Cooper (2005) demonstrate how lower crustal amphibolite dehydration melting involving plagioclase can generate and sustain radium excesses in arc magmas by incongruent continuous melting. Crystallization of feldspars within magma chambers in the shallow crust will further affect ^{226}Ra disequilibria by preferentially removing radium from melts and either reducing the magnitude of ^{226}Ra excess relative to ^{230}Th or even developing a ^{226}Ra deficit (e.g., Condomines et al., 1995; Zellmer et al., 2000).

EXPERIMENTAL METHODS

The starting composition was mixed from reagent oxides and $CaCO_3$ and ground under ethanol in an alumina mortar for five hours. The mixture was heated in air in 200°C/hour steps and held at 1000°C for 24 hours before fusing in a Pt crucible at 1450°C. The fused glass was reground under ethanol for one hour. A 0.5-gram aliquot was spiked with Ba and Sr solutions to achieve concentrations of approximately 100 ppm each. The material was dried, re-fused, and ground again under ethanol for half an hour. A fused glass of this starting composition (sample 2-1*-GL) was analyzed for major element content by electron microprobe and for Sr and Ba by SIMS. Additionally, a bead of this material, also not spiked with Ra, was run through the same experimental crystallization protocol described below, as a blank (sample 2-1*-1).

In a glove box positioned within a fume hood, approximately 2.5 μCi of ^{226}Ra in 5M HNO_3 solution was added to 150 mg of the Ba- and Sr-spiked starting material on a Teflon watch

glass. The mixture was dried under a heat lamp, formed into a bead with polyvinyl alcohol (PVA), and transferred onto a wire mesh platform ~1 cm in diameter. The bead was air-dried overnight and then placed near the top of a 1-atm Deltech vertical muffle furnace at ~170°C for four hours to ensure dryness. It was then fused for 1 hour at 1430°C and air-quenched. The glass bead material was removed from the platinum wire mesh in the glove box using a percussion mortar and tweezers. The separated glass was powdered in an agate ball mill to produce the radium-spiked starting material.

The sample charge was prepared by mixing ~30 mg of spiked starting material with a drop of PVA and adhering it to a Pt wire loop. The small bead was dried overnight at ambient temperature and transferred to the furnace, where it was subjected to a known anorthite-crystallizing thermal regime based on the procedures of Simon et al. (1994), as described in Miller et al. (2006). Since the liquidus temperature of this starting composition was approximately 1398°C (all temperatures ±5°C), the furnace was initially held at 1410°C for 1 hour to reduce potential crystal nuclei before decreasing the temperature at 2°C/hour to 1370°C, where the charge was held for 24 hours. The temperature was then decreased further at 2°C/hour until the furnace reached the final temperature of 1330°C and held there for 24 hours. The sample was air-quenched by removing it from the top of the muffle tube. The charge was mounted in Araldite epoxy and polished to 0.3 μm with alumina lapping paper before coating with carbon.

A standard (sample 2b-1-2) containing anorthite and glass of identical major element composition without radium but with elevated Ba (3000 ppm) and Sr (1000 ppm) was both quenched directly from above the liquidus to check bulk composition and also crystallized under similar experimental conditions as the radium sample and analyzed by electron microprobe at

Caltech (Miller et al., 2006). All trace element concentrations herein are expressed as oxide mole fraction (e.g. 1 ppm Ba means 1 mole BaO for every 10^6 moles of all oxide components).

SAMPLE ANALYSIS

The sample was analyzed on the modified Cameca ims-3f ion microprobe at Lawrence Livermore National Laboratory. The concentrations of ^{42}Ca, ^{88}Sr, ^{138}Ba, and ^{226}Ra were measured using a 30 μm diameter, 5 nA O^- primary beam with an impact energy of ~17 keV. Isobaric molecular interferences were minimized using energy filtering (Zinner and Crozaz, 1986); only secondary ions with kinetic energies within a 32.5 eV window centered on a 60 eV offset from the peak of the secondary ion energy distribution were focused into the mass spectrometer. Data collection consisted of 20 cycles through the mass sequence at each spot of interest, with integration times of 1 second for ^{42}Ca, ^{88}Sr and ^{138}Ba and 10 seconds for ^{226}Ra. Scans over the mass interval from 220 to 233 for both NBS-610 glass and the Ra-free anorthite/melt samples revealed virtually no background (0.2 counts/s) at mass 226. Figure 1(a) shows the portion of the mass spectrum from masses 224 to 228 on glass in the radium-free sample 2-1*-1 at 2 nA beam intensity; Figure 1(b) shows the same mass region for a radium-bearing glass sample (2-1*-Ra) at identical beam conditions. Mass scans were restricted to ±0.15 amu centered at each integer mass. Radium is clearly detected at mass 226 with average background intensity accounting for ~1 % of the Ra peak intensity in the glass over the 226 mass range shown in Figure 1.

Concentrations (C_i, ppm) were calculated by applying a calibration factor, F, to convert secondary ion intensities to ppm abundances. For Sr and Ba, these calibration factors were obtained from electron probe analysis of the standard anorthite- and glass-containing sample 2b-1-2, which was spiked with 3000 ppm Ba and 1000 ppm Sr. F values for the glass (^{88}Sr = 2900±100, ^{138}Ba = 3300±200) and anorthite (^{88}Sr = 2000±100, ^{138}Ba = 2300±400) were

calculated from ^{42}Ca-normalized ion intensities. Since no appropriate standard was available for Ra, ^{226}Ra ion intensities were converted to ppm abundances using the upper bound on the F-value for Ba. $C_{i,\,std}$ represents the concentration (ppm) of ion i in a standard and I_i is ion intensity (counts/s) in the material with unknown concentration of i:

$$F=(C_{i,\,std})\left(\frac{I_{Ca}}{I_i}\right)_{std}. \qquad (1)$$

Concentrations in the samples were determined according to the equation,

$$C_i = F\left(\frac{I_i}{I_{Ca}}\right)\left(\frac{CaO_i}{CaO_{std}}\right), \qquad (2)$$

where I_i represents the ion intensity for the element of interest in the sample, I_{Ca} is the ^{42}Ca ion intensity, CaO_i is the known CaO concentration in the sample, and CaO_{std} is the CaO concentration in the standard from which the calibration factor was established. In this case CaO_i and CaO_{std} have identical values. Following Brenan et al. (1995), the detection limit calculated for radium at mass 226 is 2 ppb for both anorthite and glass.

RESULTS AND DISCUSSION

The sample charge consisted of CMAS glass and well-formed pure anorthite laths, the largest measuring over 100 μm along its short dimension. Since the spatial resolution of our analyses is limited by the ~30 μm diameter of the ion probe primary beam, measurements were taken in the centers of crystals and assumed to represent near-liquidus growth at 1400°C. Table 1 reports molar partition coefficients for Ca, Sr, and Ba, calculated from crystal center and glass starting compositions, with uncertainties propagated from both crystal and glass analyses. Initial melt compositions used to calculate D^mMg and D^mRa (that is, mole fraction of the oxide of interest in anorthite divided by mole fraction of the oxide in the melt) were obtained by back-correcting final melt composition to account for 23% crystallization. Total fraction crystallized

was calculated using the Rayleigh equation and Ba data. The determined molar partition coefficient for Ra is 0.040±0.006.

Lattice strain modeling with D_{Ra}

The most commonly used partitioning model describing the empirical observation of a quasi-parabolic relationship between log of isovalent cation partition coefficients and ionic radii of those cations (Onuma et al., 1968) is that of Blundy and Wood (1994):

$$D_i(P,T,X) = D_o(P,T,X)\exp\left[-4\pi E N_A\left[\frac{r_o}{2}(r_i - r_o)^2 + \frac{1}{3}(r_i - r_o)^3\right] / RT\right] \quad (3)$$

Here the partition coefficient D_i for a given absolute temperature (T), pressure (P), and phase compositions (X) is a function of the ideally-sized radius (r_o) of a fictive cation with partition coefficient (D_o) that would fit into the crystallographic site without strain, the radius of the cation of interest (r_i), and a strain parameter qualitatively related to the Young's Modulus of the site (E). N_A is Avogadro's number and R is the gas constant.

The addition of radium partitioning data to a plagioclase Onuma curve for divalent cations provides a unique opportunity to test the application of lattice strain modeling to prediction of large, geologically short-lived radioactive isotope partitioning. The best-fit lattice strain model parameters for these data, when fitted in natural log space at 1400°C, are D_o = 0.93(5), r_o = 1.207(6) Å, and E = 107(9) GPa. Parameterizing with only the Ca, Sr, and Ba partition coefficients of this study (that is, excluding the Ra data) results in a 5% decrease in E with negligible changes for D_o and r_o. These r_o and E values fall within or close to the reported uncertainty of the extrapolated end-member anorthite parameters in Blundy and Wood (1994), although those authors considered all magnesium to reside in the plagioclase M site for their parameterizations.

Magnesium has been shown to occupy both tetrahedral and octahedral sites in anorthite (Longhi et al., 1976; Peters et al., 1995) and its exact site distribution in this composition remains unknown. Therefore, magnesium data are not used in the Onuma curve parameterization here, though the bulk molar distribution coefficient is plotted in Figure 2. Using the lattice strain model to predict the partitioning of octahedrally coordinated Mg in anorthite results in an estimated octahedral site occupancy of 35%, which differs from previous, significantly lower, estimates of 3% and 9% for this composition based on thermodynamic melt modeling (Miller et al., 2006).

Ra-Ba fractionation

The extent to which barium partitioning can be used to estimate initial ^{226}Ra contents of magmas prior to crystallization in magma chambers, an important component of dating eruptions, remains unresolved. Although Ra-Ba fractionation is clearly predicted by lattice strain equilibrium partitioning models, some studies continue to find assumptions of identical geochemical behavior sufficient to recover initial (^{226}Ra)/Ba ratios of magmas (e.g., Condomines et al., 2005). We measure a D_{Ra}/D_{Ba} of 0.23±0.05 for this composition, which compares favorably with estimates of 0.21-0.25 for plagioclase used by other workers (Cooper and Reid, 2003; Cooper et al., 2001). Greater D_{Ra}/D_{Ba} fractionation, characterized by a tighter Onuma curve, results with increased Ca content in plagioclase and/or decreased temperature (Cooper et al., 2001). Although this study was conducted at 1400°C, strain modeling using the parameters reported here permits calculating Ra-Ba fractionation between highly calcic plagioclases and melt at the lower temperatures more common in natural environments.

Implications for radium partitioning in clinopyroxene

($^{226}Ra/^{230}Th$) excesses in young volcanic rocks are ubiquitous across a wide range of geologic environments and range from slight in OIB settings to values of over 6 in some arc lavas (Turner et al., 2001). While fluid addition is also implicated in arc settings, such excesses are generally thought to result from Ra-Th fractionation during melting and to be preserved by rapid transport of the melt to the surface, although the exact location of radium excess production in even the relatively uncomplicated MOR setting remains an open question. A study of well-characterized lavas from the East Pacific Rise (Sims et al., 2002) attributed the inverse ^{226}Ra and ^{230}Th excess systematics to polybaric melting of a homogenous source, with the ^{226}Ra excesses generated at shallower depths in equilibrium with depleted spinel harzburgite material just beneath the lower crust.

The dominant mantle reservoir of radium below the plagioclase peridotite field is likely clinopyroxene, except possibly in hydrous environments where phases such as phlogopite (calculated $D_{Ra} > 1$ for melts and >>1 for fluids) may play a significant role in radium storage at depth (Feineman and DePaolo, 2003). Given that Ra^{2+} has been shown here to be a well-behaved ion whose partitioning behavior between plagioclase and melt is closely approximated by a lattice strain partitioning model (Blundy and Wood, 1994), this study lends further confidence to clinopyroxene/melt D_{Ra} estimates, typically on the order of 10^{-7} (Cooper et al., 2003), calculated from such models.

CONCLUSIONS

For the first time, experimental radium partitioning data are available to test a widely-used predictive partitioning model (Blundy and Wood, 1994). Hitherto, Ra partitioning behavior has been estimated or calculated rather than directly measured. When focus is restricted to

divalent elements known enter only the 7-fold site in anorthite (Ca, Sr, Ba, Ra), we find excellent agreement of the measured radium partition coefficients with those predicted by lattice strain models. Our results show that partitioning studies for phases in which Ra is more compatible, such as potassium feldspars and phlogopite (Blundy and Wood, 2003), could be relatively straightforward. Furthermore, our present experiments have sufficient analytical margins that obtaining Ra partition coefficients at least one and possibly two orders of magnitude lower would be feasible.

Acknowledgements: The authors wish to thank Haick Issaian and Andre Jefferson of the Caltech Safety Office for their time and expertise in assisting with safe handling of materials. NORIT Americas, Inc. generously donated activated charcoal for radon containment. This work was supported by NASA grants NAG5-11640 and NNG05GH79G to D. Burnett, NSF EAR-0239513 to P. Asimow and LLNL Laboratory Directed Research and Development funding. This work was performed under the auspices of the U.S. Department of Energy by the University of California, Lawrence Livermore National Laboratory under Contract W-7405-Eng-48.

References

Blundy, J., and Wood, B. (1994) Prediction of crystal-melt partition coefficients from elastic moduli. Nature, 372, 452-454.

-. (2003) Mineral-melt partitioning of uranium, thorium and their daughters. In B. Bourdon, G.M. Henderson, C.C. Lundstrom, and S.P. Turner, Eds. Uranium-series geochemistry, 52, p. 59-123. Mineralogical Society of America.

Brenan, J.M., Shaw, H.F., Ryerson, F.J., and Phinney, D.L. (1995) Mineral-aqueous fluid partitioning of trace elements at 900°C and 2.0GPa: constraints on the trace element chemistry of mantle and deep crustal fluids. Geochimica et Cosmochimica Acta, 59, 3331-3350.

Condomines, M., Gauthier, P.J., Tanguy, J.C., Gertisser, R., Thouret, J.C., Berthommier, P., and Camus, G. (2005) ^{226}Ra or ^{226}Ra/Ba dating of Holocene volcanic rocks: application to Mt. Etna and Merapi volcanoes. Earth and Planetary Science Letters, 230, 289-300.

Condomines, M., Tanguy, J.-C., and Michaud, V. (1995) Magma dynamics at Mt. Etna: constraints from U-Th-Ra-Pb radioactive disequilibria and Sr isotopes in historical lavas. Earth and Planetary Science Letters, 132, 25-41.

Cooper, K.M., Goldstein, S.J., Sims, K.W.W., and Murrell, M.T. (2003) Uranium-series chronology of Gorda Ridge volcanism: new evidence from the 1996 eruption. Earth and Planetary Science Letters, 206, 459-475.

Cooper, K.M., and Reid, M.R. (2003) Re-examination of crystal ages in recent Mount St. Helens lavas: implications for magma reservoir processes. Earth and Planetary Science Letters, 213, 149-167.

Cooper, K.M., Reid, M.R., Murrell, M.T., and Clague, D.A. (2001) Crystal and magma residence at Kilauea Volcano, Hawaii: ^{230}Th-^{226}Ra dating of the 1955 east rift eruption. Earth and Planetary Science Letters, 184, 703-718.

Dufek, J., and Cooper, K.M. (2005) ^{226}Ra/^{230}Th excess generated in the lower crust: implications for magma transport and storage time scales. Geology, 33, 833-836.

Feineman, M.D., and DePaolo, D.J. (2003) Steady-state ^{226}Ra/^{230}Th disequilibrium in mantle minerals: implications for melt transport rates in island arcs. Earth and Planetary Science Letters, 215, 339-355.

Longhi, J., Walker, D., and Hays, J. (1976) Fe and Mg in plagioclase. Seventh Lunar Science Conference, p. 1281-1300.

Miller, S.A., Asimow, P.D., and Burnett, D.S. (2006) Determination of melt influence on divalent element partitioning between anorthite and CMAS melts. Geochimica et Cosmochimica Acta, 70, 4258-4274.

Onuma, N., Higuchi, H., Wakita, H., and Nagasawa, H. (1968) Trace element partitioning between two pyroxenes and the host lava. Earth and Planetary Science Letters, 5, 47-51.

Peters, M.T., Shaffer, E.E., Burnett, D.S., and Kim, S.S. (1995) Magnesium and titanium partitioning between anorthite and Type B CAI liquid: dependence on oxygen fugacity and liquid composition. Geochimica et Cosmochimica Acta, 59, 2785-2796.

Presnall, D.C., Gudfinnsson, G.H., and Walter, M.J. (2002) Generation of mid-ocean ridge basalts at pressures from 1 to 7 GPa. Geochimica et Cosmochimica Acta, 66, 2073-2090.

Reagan, M.K., Volpe, A.M., and Cashman, K.V. (1992) ^{238}U- and ^{232}Th-series chronology of phonolitic fractionation at Mount Erebus, Antarctica. Geochimica et Cosmochimica Acta, 56, 1401-1407.

Saal, A.E., and Van Orman, J.A. (2004) The ^{226}Ra enrichment in oceanic basalts: evidence for melt-cumulate diffusive interaction processes within the oceanic lithosphere. G^3, 5, doi:10.1029/2003GC000620.

Schaefer, S.J., Sturchio, N.C., Murrell, M.T., and Williams, S.N. (1993) Internal ^{238}U-series systematics of pumice from the November 13, 1985 of Nevado del Ruiz, Columbia. Geochimica et Cosmochimica Acta, 57, 1215-1219.

Shannon, R.D. (1976) Revised effective ionic radii and systematic studies of interatomic distances in halides and chalcogenides. Acta Crystallographica, A 32, 751-767.

Simon, S.B., Kuehner, S.M., Davis, A.M., Grossman, L., Johnson, M.L., and Burnett, D.S. (1994) Experimental studies of trace element partitioning in Ca, Al-rich compositions: anorthite and perovskite. Geochimica et Cosmochimica Acta, 58, 1507-1523.

Sims, K.W.W., Goldstein, S.J., Blinchert-Toft, J., Perfit, M.R., Kelemen, P., Fornari, D.J., Michael, P., Murrell, M.T., Hart, S.R., DePaolo, D.J., Layne, G., Ball, L., Jull, M., and Bender, J. (2002) Chemical and isotopic constraints on the generation and transport of magma beneath the East Pacific Rise. Geochimica et Cosmochimica Acta, 66, 3481-3504.

Turner, S., Evans, P., and Hawkesworth, C. (2001) Ultrafast source-to-surface movement of melt at island arcs from ^{226}Ra-^{230}Th systematics. Science, 292, 1363-1366.
Van Orman, J.A., Saal, A.E., Bourdon, B., and Hauri, E.H. (2006) Diffusive fractionation of U-series radionuclides during mantle melting and shallow-level melt-cumulate interaction. Geochimica et Cosmochimica Acta, 70, 4797-4812.
Volpe, A.M., and Hammond, P.E. (1991) ^{238}U-^{230}Th-^{226}Ra disequilibrium in young Mount St. Helens rocks: time constraint for magma formation and crystallization. Earth and Planetary Science Letters, 107, 475-486.
Zellmer, G., Turner, S., and Hawkesworth, C. (2000) Timescales of destructive plate margin magmatism: new insights from Santorini, Aegean volcanic arc. Earth and Planetary Science Letters, 174, 265-281.
Zinner, E. and Crozaz, G. (1986) A method for the quantitative measurement of rare earth elements in the ion microprobe. Intl. J. Mass Spec. Ion Proc., 69, 17-38.

Captions:

Table 1. Compositions of starting material, Ba and Sr standard, radium-free sample, and radium-bearing sample as determined by electron microprobe (EMP, reported in weight percent) and ion microprobe (SIMS, reported in weight parts per million) analysis. Elements not analyzed denoted by '-'. Na_2O, K_2O, FeO (total iron as FeO) were analyzed by EMP in standard sample 2b-1-2 and found to be 0.02 wt. % or less. Molar partition coefficients for divalent elements are reported for data collected from centers of crystals and random surrounding glass points back-corrected for fractional crystallization to initial melt composition. Standard deviation (1σ) in the last one or two decimal places is given by the numbers in parentheses.

Figure 1. SIMS mass spectra of the region surrounding mass 226 for (a) glass of the radium-free sample 2-1*-1 and (b) glass of the radium-bearing sample 2-1*-Ra. Data were collected over a ±0.15 amu interval centered at each integer mass with ion intensities measured every 0.010 amu. Secondary ion intensity is reported in counts per second.

Figure 2. Onuma curve generated by lattice strain modeling of Ca, Sr, Ba, and Ra molar partition coefficients. Ionic radii are for VIII-fold coordination taken from Shannon (1976). Uncertainties are reported as 1σ and are within the size of the markers except where explicitly shown. Partition coefficient for total Mg is shown, but this point is not used in fitting, since an unknown fraction of the Mg in anorthite is on a different site (see text).

Table 1.

	EMP (wt. %)			SIMS (ppm)			
	Starting glass 2-1*-GL n = 4	Standard 2b-1-2 Anorthite n = 10	Standard 2b-1-2 Glass n = 10	Ra-free Run 2-1*-1 Anorthite	Ra-free Run 2-1*-1 Glass	Run 2-1*-Ra Anorthite	Run 2-1*-Ra Glass
SiO_2	46.6 (2)	43.4 (1)	47.97 (11)	-	-	-	-
Al_2O_3	21.56 (6)	36.5 (2)	18.14 (19)	-	-	-	-
MgO	0.99 (1)	0.099 (4)	1.19 (6)	-	-	-	-
CaO	30.26 (7)	20.9 (1)	32.48 (18)	-	-	-	-
SrO	114 (4) †	0.111(5)	0.136 (5)	99 (5)	111 (4)	96 (5)	112 (4)
BaO	68 (4) †	0.097 (8)	0.60 (3)	10 (2)	76 (4)	12 (2)	85 (5)
RaO	nd †	--	--	nd	nd	0.16 (3)	5.2 (3)

	$D^{m}Mg$**	$D^{m}Ca$	$D^{m}Sr$	$D^{m}Ba$	$D^{m}Ra$
2-1*-Ra	0.098 (6)	0.724 (4)	0.84 (6)	0.17 (3)	0.040 (6)

nd = not detected

† Doping concentrations (ppm) as measured by SIMS on quenched glass of starting material.

** Bulk Mg partition coefficient shown from standard run 2b-1-2, including all magnesium in anorthite, irrespective of crystal coordination environment.

Figure 1.

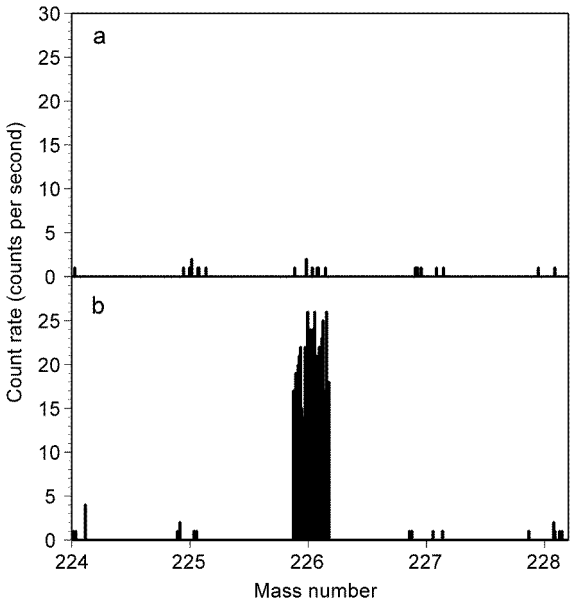
a
b
Count rate (counts per second)
Mass number
0
5
10
15
20
25
30
224
225
226
227
228

Figure 2.

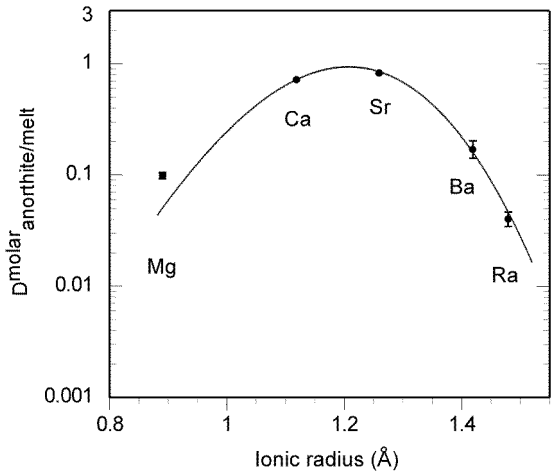
3
1
0.1
0.01
0.001
$D^{molar}_{anorthite/melt}$
Mg
Ca
Sr
Ba
Ra
0.8
1
1.2
1.4
Ionic radius (Å)